Preprint Title	Supramolecular hydration structure of graphene-based hydrogels: density functional theory, green chemistry and interface application
Authors	Hon Nhien Le, Duy Khanh Nguyen, Minh Triet Dang, Huyen Trinh Nguyen, Thi Bang Tam Dao, Trung Do Nguyen, Chi Nhan Ha Thuc and Van Hieu Le
Publication Date	21 Jan. 2025
Article Type	Full Research Paper
Supporting Information File 1	Supporting_Information_Preliminary Revision.docx; 4.2 MB
ORCID® iDs	Hon Nhien Le - https://orcid.org/0000-0001-5397-7665; Minh Triet Dang - https://orcid.org/0000-0003-1769-4873

Supramolecular hydration structure of graphene-based hydrogels: density functional theory, green chemistry and interface application

Hon Nhien Le*[1,4], Duy Khanh Nguyen[5,6], Minh Triet Dang[7], Huyen Trinh Nguyen[3,4], Thi Bang Tam Dao[1,4], Trung Do Nguyen[1,4], Chi Nhan Ha Thuc*[1,4] and Van Hieu Le*[1,2,4]

Address: [1]Faculty of Materials Science and Technology, University of Science, Ho Chi Minh City, 700000, Vietnam, [2]Faculty of Chemistry, VNUHCM University of Science, 227 Nguyen Van Cu Street, Ward 4, District 5, Ho Chi Minh City, 700000, Vietnam, [3]Multifunctional Materials Laboratory, VNUHCM University of Science, 227 Nguyen Van Cu Street, Ward 4, District 5, Ho Chi Minh City, 700000, Vietnam, [4]Vietnam National University, Linh Trung Ward, Thu Duc City, Ho Chi Minh City, 700000, Vietnam, [5]Laboratory for Computational Physics, Institute for Computational Science and Artificial Intelligence, Van Lang University, Ho Chi Minh City, 700000, Vietnam, [6]Faculty of Mechanical – Electrical and Computer Engineering, School of Technology, Van Lang University, Ho Chi Minh City, 700000, Vietnam and [7]Faculty of Physics, School of Education, Can Tho University, Can Tho City, Viet Nam

Email: Hon Nhien Le - lhnhien@hcmus.edu.vn

Chi Nhan Ha Thuc - htcnhan@hcmus.edu.vn

Van Hieu Le - lvhieu@hcmus.edu.vn

* Corresponding author

Abstract

Natural hydration shells are discovered to play an essential role in the structure and function of biomolecules (deoxyribonucleic acid, protein and phospholipid membrane). Hydration layers are also important to the structure and property of artificial graphene-based materials. Our recent researches prove that graphene-based hydrogels are supramolecular hydration structures that preserve graphene nanosheets from irreversible stacking via van der Waals forces and π-π interactions. In this manuscript, density functional theory (DFT) and high performance computing (HPC) are used for modeling and calculating van der Waals force between graphene nanosheets in water-intercalated AB bilayer graphene structures. A layer of water molecules significantly decreases the intersheet van der Waals force. Experimentally, a novel hydrogel of graphene oxide – silica gel – zinc hydroxide (GO-SG-ZH) is synthesized to demonstrate the advantages of hydrated hydrogel structure in comparison with dry powder structure. The synthesis of graphene-based hydrogels is a green chemistry approach to attain extraordinary properties of graphene-based nanostructures. Hydration forces in the hydrogel prevent van der Waals stacking and graphene agglomeration. Analytical characterizations exhibited moisture contents, three-dimensional structures, elemental compositions, functional groups and antibacterial activities. Non-stacking state of graphene-based nanosheets in GO-SG-ZH hydrogel was suitable for direct brush painting on polymer substrates, typically polylactide films. GO-SG-ZH coating on polylactide film was antibacterial and stable in aqueous food simulants for one month. In general, supramolecular graphene-based hydrogels are bioinspired hydration structures to advance nanoscale properties and nanotechnology applications.

Keywords

graphene-based hydrogel; bioinspired hydration; supramolecular structure; density functional theory; antibacterial coating

Introduction

Natural biological cells are wonderful assemblies of biomolecules that are hydrated with water molecules. Cell content includes about 70 – 95% water that creates aqueous environment for biological processes. Water molecules are bound to biomolecular surfaces and participate in the structuring and functioning of biomolecules, typically the folding of protein and the twisting of deoxyribonucleic acid (DNA) double helix [1]. Water molecules and their hydrogen bonding network function as lubricants for biomolecular dynamics. Recent scientific researches analyzed the important role of hydration shells on DNA, proteins and phospholipid membranes [2-4]. The first hydration shell (about 3.5 Å) at the interface of biomolecules has considerably slower dynamics than water molecules in the bulk. Besides, the first water layer on the interface is responsible for hydration forces between biomolecular structures [5]. The rearrangement of water molecules through hydrogen bonding on hydrated surfaces generates repulsive hydration forces when another surface perturbs the hydration layers [6-8]. Hydration shells and hydration forces keep the hydrated structures stable and functional in the natural concert of biological processes.

In the aspect of artificial nanomaterials, it is proposed that hydration also plays an important role in the stability and functionality of nanoscale structures. Van der Waals force is a main intermolecular interaction that governs the agglomeration of nanomaterials. Carbon nanostructures with π-conjugated systems (fullerene, carbon nanotube and graphene) have π-π interactions, a type of van der Waals force, for

supramolecular attraction [9]. Particularly, graphene sheets with large surface area and π-conjugated network are likely to stack together through hydrophobic agglomeration and π-π interaction. Strong binding energy of van der Waals force may cause irreversible graphene stacking. The stacking of graphene-based nanosheets, typically pristine graphene, graphene oxide (GO) and reduced graphene oxide (RGO), brings about small effective surface area and low dispersibility in media [10]. Several approaches have been reported to prevent the irreversible stacking of graphene-based nanosheets, including electrostatic charge, nanoparticle intercalation, three-dimensional assembly and surface hydration [10-12]. In our previous researches, a number of graphene-based hydrogels (RGO-SnO_2, RGO-ZnO and RGO) were synthesized to evidence the reversible self-assembly of graphene-based nanosheets thanks to water intercalation in the hydrated ensembles [13-17]. Therefore, supramolecular graphene-based hydrogels with hydration swelling and hydration force are quite useful for preserving and generating graphene-based nanosheets for many applications.

In this manuscript, we calculated van der Waals forces in bilayer graphene structures using density functional theory modeling (DFT) and dispersion energy correction functional (DFT-D3). The theoretical work aimed to elucidate the relationship between water intercalation and intersheet binding energy in quantum mechanical level. The computational calculations quantified intersheet distance, van der Waals force, band gap energy and formation energy of the molecular system of bilayer graphene intercalated with a water layer. In experimental aspect, green chemistry methods were applied for synthesizing GO nanosheets, rice husk silica gel (SG), zinc hydroxide nanoparticles (ZH) and graphene oxide – nanosilica – zinc hydroxide nanocomposites (GO-SG-ZH). Graphite oxidation reaction in a cascade design gives good efficiencies of energy, chemical and time [14,15]. The recycling of rice husk ash waste into

nanosilica products is eco-friendly and sustainable for circular economy [18-21]. Especially, GO nanosheets decorated with SG and ZH nanoparticles have hydrophilic surfaces to retain hydration layers in the hydrogel structure of GO-SG-ZH nanocomposite. Hydration layers in GO-SG-ZH hydrogel also function as lubricants at the nanomaterials interfaces, leading to facile brush coating on plastic films of polylactide (PLA). Dehydrated GO-SG-ZH coating adhered to the PLA substrate through van der Waals interaction. Furthermore, antibacterial activities, interfacial stability, mechanical properties of the nanocomposite materials were analyzed and described in the results and discussion.

Methods

Computation method of density functional theory

First-principles calculations based on density functional theory (DFT) were conducted using the Vienna ab initio simulation software (VASP) and a high performance computing system (HPC). Projector augmented wave method (PAW) was implemented in the electronic structure calculations. Generalized gradient approximation of Perdew–Burke–Ernzerhof (GGA-PBE) was used for describing exchange-correlation energy of electron-electron interaction. The correction of van der Waals dispersion energy was applied using DFT-D3 method proposed by S. Grimme [22-24]. The modeling of infinite graphene sheets was extrapolated from periodic supercells. The supercell of bilayer graphene structure includes 16 carbon atoms (2 graphene sheets with 8 carbon atoms per sheet). The modeling of water-intercalated bilayer graphene structure used the supercell of 16 carbon atoms, 1 oxygen atom and 2 hydrogen atoms (2 graphene sheets and 1 water molecule).

Preparation of graphene oxide from natural graphite

The improved cascade-design synthesis of graphite oxide (GrO) was reported in our previous papers [15,16]. Briefly, 5 g raw material of natural graphite (Shanghai Zhanyun Chemical) was soaked and agitated in 50 mL sulfuric acid 98%. The solution of Mn(VII) compound was prepared by dissolving 10 g potassium permanganate in 100 mL sulfuric acid 98%. The graphite/H_2SO_4 suspension was slowly poured into the Mn(VII) solution. A cooling water bath and an infrared thermometer were used for controlling the reactor temperature below 55^oC (the peak of reactor temperature is about 50^oC). After agitation in room condition for 4 hours, the graphite/Mn(VII)/H_2SO_4 suspension was slowly poured into 360 mL water (exothermic heat made the reactor temperature above 90^oC). After 2-hours agitation, the reaction was mixed with 150 mL H_2O_2 solution 5% and kept stirring for 1 day. After washing to neutral pH, obtained material was dried and ground to produce a GrO powder (moisture ~ 20%). Next, GrO powder was dispersed in water and sonicated for 1 hour. After natural sedimentation over night, the suspension was decanted to collect the supernatant dispersion of GO nanosheets.

Preparation of nanosilica from rice husk ash waste

Rice husk ash that was discarded from industrial boilers was collected for recycling experiments. Our method of nanosilica synthesis using potassium hydroxide and acetic acid was mentioned in a recent paper [21]. Raw material of rice husk ash waste was dispersed in a potassium hydroxide solution 7%. The suspension was agitated for 1 hour at temperature of 80 – 90^oC. After carefull filtration, a clear yellow solution of potassium silicate was obtained and neutralized with acetic acid solution 15%. After that, the suspension of precipitated nanosilica was incubated over night and then

washed thoroughly with water. Obtained product of silica gel (SG) was used for subsequent synthesis and brush coating experiments.

Synthesis of graphene oxide – nanosilica – zinc hydroxide hydrogel

The suspension of 0.625 g GrO and 250 mL water was agitated and then sonicated for 1 hour. The suspension was left over night and decanted to collect about 250 mL GO dispersion. 4.4 g $Zn(CH_3COO)_2.2H_2O$ was dissolved in 250 mL water to prepare 250 mL Zn^{2+} solution. The Zn^{2+} solution was dropped slowly into the GO solution under stirring. Obtained GO/Zn^{2+} dispersion was sonicated for 30 minutes. Besides, 20 g SG material (moisture ~ 95%) was mechanically dispersed in 480 mL water for 15 minutes and then sonicated for 15 minutes. 500 mL as-prepared GO/Zn^{2+} dispersion was dropped into the 500 mL SG dispersion. The mixture was agitated for 15 minutes and sonicated for 15 minutes. Then, the reaction was adjusted to pH 10 using ammonia solution for $Zn(OH)_2$ precipitation and kept stirring for 1 hour. After sedimentation, the material was filtered and washed with excessive water. A hydrogel of graphene oxide – nanosilica – zinc hydroxide (GO-SG-ZH hydrogel) was collected and analyzed.

To produce a GO-SG-ZH product in powder form, GO-SG-ZH hydrogel was dried at 80^oC and ground to obtain GO-SG-ZH powder. The graphene-based nanocomposites in hydrogel form and in powder form were characterized comparatively using moisture analysis, scanning electron microscopy (SEM), energy-dispersive X-ray spectroscopy (EDS) and aqueous dispersibility.

Brush coating of graphene oxide – nanosilica – zinc hydroxide hydrogel on polylactide film

At first, commercial polylactide granules (PLA Luminy LX175, TotalEnergies Corbion) was put in a steel mold for thermal compression at 190^oC to produce a PLA plate. A

piece of the PLA plate was put in a thin plastic mold (polyethylene terephthalate) for thermal compression at 190^{o}C. A a result, thin and transparent PLA films were made with the average thickness of 0.2 mm.

In the next stage, GO-SG-ZH nanocomposite in hydrogel form (~ 95% water) was used as an aqueous paint for brush coating on PLA thin films. After brush coating, the coated films were left for air drying in 3 hours and mildly dried using a hair dryer. Obtained coated films were denoted as GO-SG-ZH/PLA. Besides, as-synthesized SG hydrogel (~ 95% water) was also suitable for direct brush coating on PLA films. Similar procedure of brush coating was applied to produce PLA thin films coated with nanosilica. The nanosilica-coated films were denoted as SG/PLA.

Materials characterizations

Materials weights and moistures were measured using a laboratory balance (Ohaus Pioneer, 220 g/0.0001 g) and a moisture analyzer (A&D Weighing MX-50, 51 g/0.001 g). Scanning electron microscopy (SEM) and energy-dispersive X-ray spectroscopy (EDS) were was analyzed using a JSM-IT200 system (JEOL). Samples were coated with Pt before SEM-EDS analysis. X-ray diffraction (XRD) was scanned by a D8 Advance instrument (Bruker). Fourier transform infrared spectroscopy (FTIR) was characterized with a FT/IR-6600 instrument (Jasco). Ultraviolet-visible absorption spectroscopy (UV-Vis) and light transmittance spectroscopy were recorded using a V-670 spectrophotometer (Jasco). Microscopic texture and imaging were observed by a stereo zoom microscope (Optika SZM). Agar well diffusion assay was used for testing antibacterial activity against *E. coli* and *S. aureus* bacteria (the positive control is penicillin antibiotic). Inhibition zone assay was tested for evaluating antibiofilm property of uncoated and coated plastic films [14,25]. Coating stability of plastic films in aqueous food simulants was experimented using the method reported in our previous paper

[14,26]. Measurement of tensile properties was conducted using an universal tensile testing machine (Yang Yi Technology, 500-N load cell) and the standard of ASTM D882-18 [14,27].

Results and Discussion

Density functional theory calculations of intersheet distances, van der Waals forces and band gaps

Van der Waals force, particularly π- π interaction, is responsible for the restacking of graphene sheets. In drying condition, as solvation shells of graphene sheets are removed, the distance between graphene sheets becomes closer and the interaction surface area is larger. At short intersheet distances, van der Waals force may increase to a high binding energy that accounts for the so-called irreversible stacking of graphene sheets. The issue of graphene restacking at dry state is the main cause of lower dispersibility and surface area of graphene-based materials in many applications, such as aqueous dispersions, polymer nanocomposites and aqueous paints. Our previous researches demonstrated that in graphene-based hydrogel structures, the intercalation of water molecules between graphene-based sheets maintains large intersheet distances and low interaction surface area, which leads to reduced binding energy of van der Waals force [14,15]. The simple method of water intercalation in hydrogel structures is an effective bioinspired approach to prevent nanosheet stacking and preserve graphene-based nanostructures.

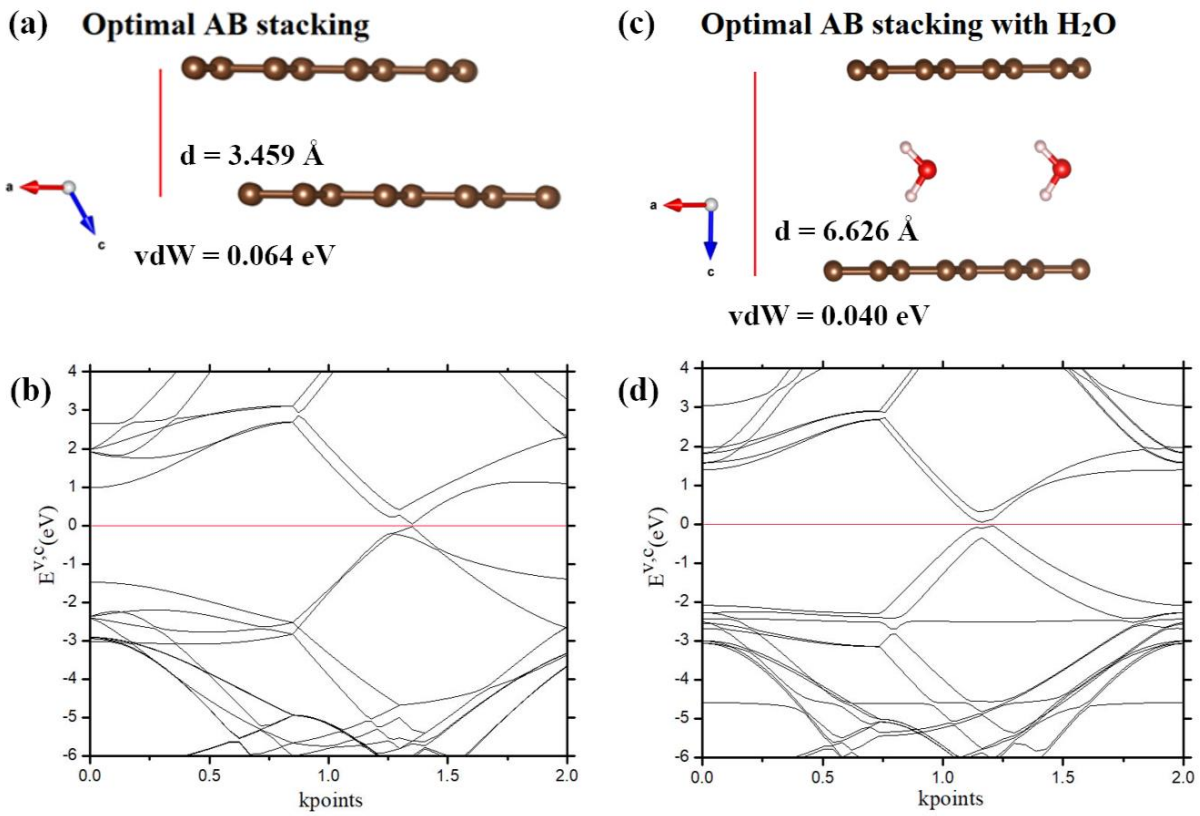

Figure 1: DFT modeling of AB bilayer graphene structures. The AB bilayer graphene with the intersheet distance of 3.459 Å (a), and its valence – conduction band structure in hexagonal Brillouin zone (b). The AB bilayer graphene structure intercalated with a layer of water molecules and the intersheet distance of 6.626 Å (c), and its electronic band structure in hexagonal Brillouin zone (d).

Herein, DFT calculations were performed to quantify the van der Waals dispersion interactions in pristine bilayer graphene and water-intercalated bilayer graphene structures. In natural multilayer graphite, graphene sheets stack together in AB configuration. Figure 1a shows the modeling of a bilayer graphene structure that mimics the AB stacking in multilayer graphite. DFT optimization calculation presented that pristine bilayer graphene has the formation energy of -9.3778 eV/supercell, intersheet distance of 3.459 Å and van der Waals binding energy of 0.064 eV/atom (Figure 1b and Table 1). The intersheet distance is comparable with the values reported in other papers [28-30]. The bilayer graphene structure has a small band gap

of 0.064 eV/atom that is slightly opened in comparison with the zero band gap of a single-layer graphene sheet.

Table 1: Formation energies, intersheet distances, van der Waals forces and band gaps of bilayer graphene structures.

Configuration	Formation energy (eV)	C-C bond length (Å)	Intersheet distance (Å)	Van der Waals force (eV)	Band gap (eV)
Pristine AB bilayer graphene	-9.3778	1.42	3.459	0.064	0.06
AB bilayer graphene intercalated with a water layer	-10.6414	1.42	6.626	0.040	0.09

Besides, DFT modeling of the water-intercalated AB bilayer graphene structure was also calculated by HPC. The resulting formation energy is -10.6414 eV/supercell (Table 1). In the optimal structure (Figures 1c and 1d), hydrogen atoms of the water molecule are oriented toward graphene sheets due to the hydrogen-π interaction. It is noteworthy that the enlarged intersheet distance of 6.626 Å led to the intersheet binding energy of 0.04 eV/atom. A layer of water molecules in between two graphene sheets significantly gave the decline of the van der Waals force by 37.5% (from 0.064 eV to 0.040 eV). The band gap of the water-intercalated bilayer graphene structure increased to 0.09 eV. Although the opening of band gap is still small, it is suggested that the band gap of AB bilayer graphene can be further opened by increasing molecular water layers in the intersheet gallery as well as the spacing distance. The approach of water intercalation in graphene-based structures is effective for lowering van der Waals force and opening band gap. Therefore, water-intercalated structures

of graphene-based nanosheets should be synthesized experimentally to ameliorate the nanostructures and properties for various applications in science and industry.

Supramolecular hydration structure of graphene oxide – nanosilica – zinc hydroxide hydrogel

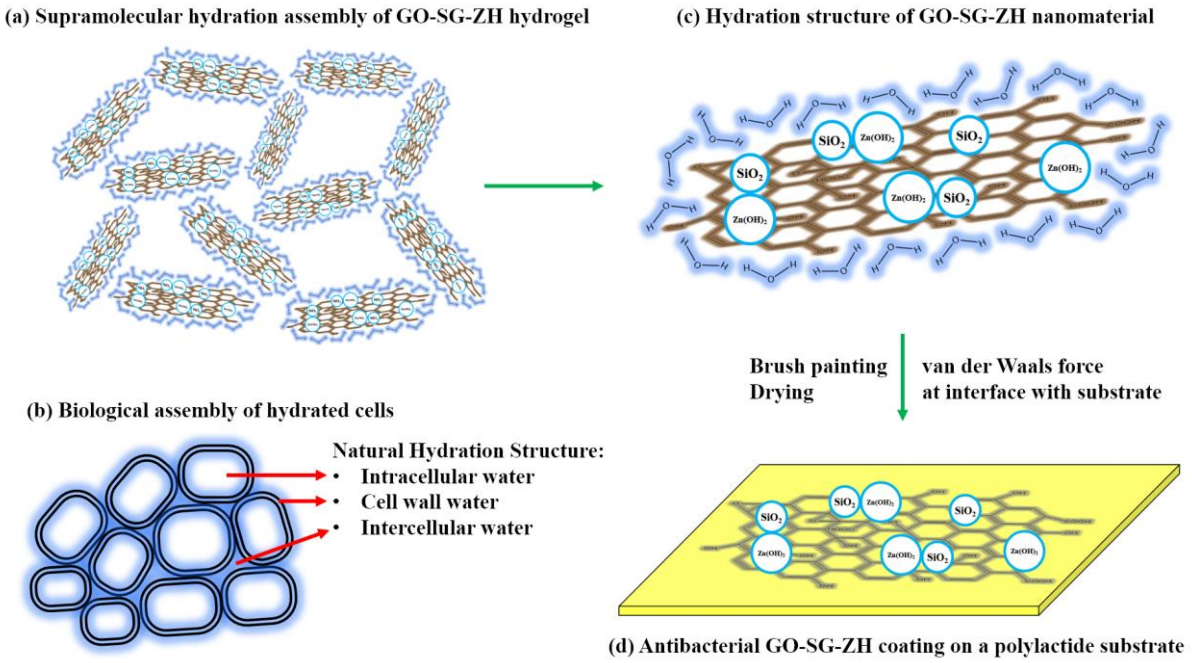

Figure 2: (a) Illustration of a supramolecular self-assembly of GO-SG-ZH hydrogel. (b) Depiction of a natural assembly of biological cells stabilized by hydration structures (water molecules on cell wall membranes are highlighted with blue color). (c) Drawing of a synthetic graphene-based nanosheets (GO-SG-ZH) covered by a hydration shell. (d) Presentation of a graphene-based coating (antibacterial GO-SG-ZH) that adheres to a substrate (PLA film).

The computational DFT results confirm the importance of supramolecular interaction of water intercalation in graphene-based structures. In this research, we synthesized the graphene-based hydrogel of graphene oxide – nanosilica – zinc hydroxide nanocomposite (GO-SG-ZH hydrogel) as a supramolecular hydration structure. Figure 2a describes the supramolecular hydration assembly of GO-SG-ZH hydrogel. GO

nanosheets have brown color, and the hydration shells of water molecules is highlighted with blue color. Hydrophilic functional groups on GO nanosheets, SG nanoparticles and ZH nanostructures are attractive to water molecules to form hydration shells on the surfaces. In addition to hydration layers, the three-dimensional assembly of graphene-based nanosheets provides high porosity as water reservoirs that supply water to intersheet galleries. High water content and large spacing distance in the hydrogel structure are key factors that prevent van der Waals and π-π interactions between graphene-based sheets.

Figure 2b depicts the hydrated assembly of biological cells in nature. The natural hydrated structure includes intracellular water, cell wall water and intercellular water [31]. Hydration shells on the cellular walls or biomembranes are important to maintain the cellular shapes. The first bound water molecules on the biomembranes is a biointerfacial water layer (~ 2.6 Å) that is responsible for primary hydration force [32-36]. Hydration forces in the range of 4 – 5 water layers contribute repulsive energy to the biological system. Supramolecular hydrogen bonding of biostructures and water molecules is attributed to the repulsive hydration forces. The artificial structure of graphene-based hydrogel in Figure 2a is biomimetic to the natural system of biological cells described in Figure 2b. Hydration shells on GO-SG-ZH nanosheets, particularly the first interfacial water layer, generate hydration forces to maintain intersheet distances and nanoscale structures in the artificial system. Drawing in Figure 2c is the presentation of a graphene-based nanosheet with a first bound water layer that would be responsible for primary hydration force. In the next stage, after brush coating of GO-SG-ZH hydrogel on a polylactide film, hydration shells are evaporated in drying process, and the graphene-based nanosheets adhere to the substrate through van der Waals interaction (Figure 2d). Hydration force and van der Waals force can be utilized for repulsion or adhesion at the interface.

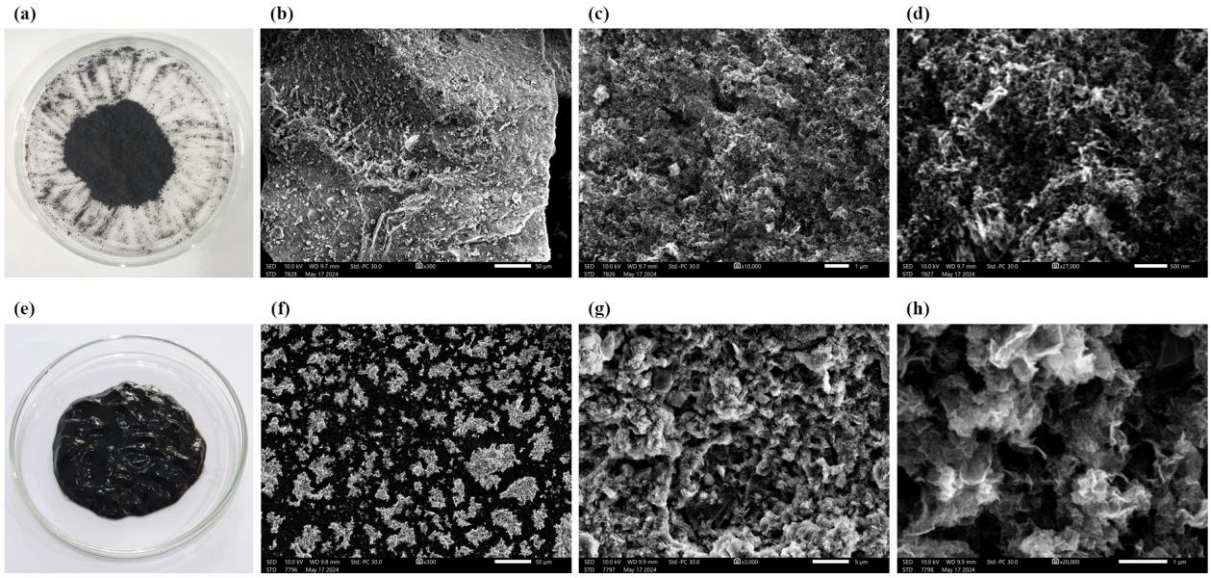

Figure 3: (a) Powder of graphene oxide – nanosilica – zinc hydroxide (GO-SG-ZH powder). SEM images showing particles and nanostructures in GO-SG-ZH powder with the scale bars of 50 µm (b), 1 µm (c) and 500 nm (d). (e) Hydrogel of graphene oxide – nanosilica – zinc hydroxide (GO-SG-ZH hydrogel). SEM images showing micro- and nano- structures in GO-SG-ZH hydrogel with the scale bars of 50 µm (f), 5 µm (g) and 1 µm (h).

Experimentally, artificial nanomaterials of GO-SG-ZH powder and hydrogel were prepared for comparative study (Figure 3). While GO-SG-ZH powder is a dry solid, GO-SG-ZH hydrogel has the moisture content of 95%. The moisture content of GO-SG-ZH hydrogel is comparable with those of natural cellular systems (moisture content of apple tissues is about 90%) [31]. Figures 3a – 3d show the macroscopic picture and microscopic images of GO-SG-ZH powder (moisture ~ 10%). Since the material was dehydrated, graphene-based nanostructures could be covalently crosslinked through esterification reaction of carboxyl and hydroxyl groups on GO nanosheets [37]. GO-SG-ZH nanosheets agglomerated and stacked together to form big particles (size of hundreds of micrometer, Figure 3b). The GO-SG-ZH particles had low porosity or small spacing among graphene-based nanosheets (Figures 3c and 3d). Besides, GO-SG-

ZH hydrogel was spread on a carbon tape for SEM imaging (Figures 3e – 3h). After water evaporation, GO-SG-ZH nanosheets agglomerated into microstructures (Figure 3f), and the self-assembly of the nanomaterials was different from the morphology of powder agglomeration. At higher manifications, SEM images in Figures 3g and 3h revealed the porous morphology with large spacing among graphene-based nanosheets. As a result, GO-SG-ZH hydrogel is a three-dimensional assembly of water-intercalated graphene-based nanosheets.

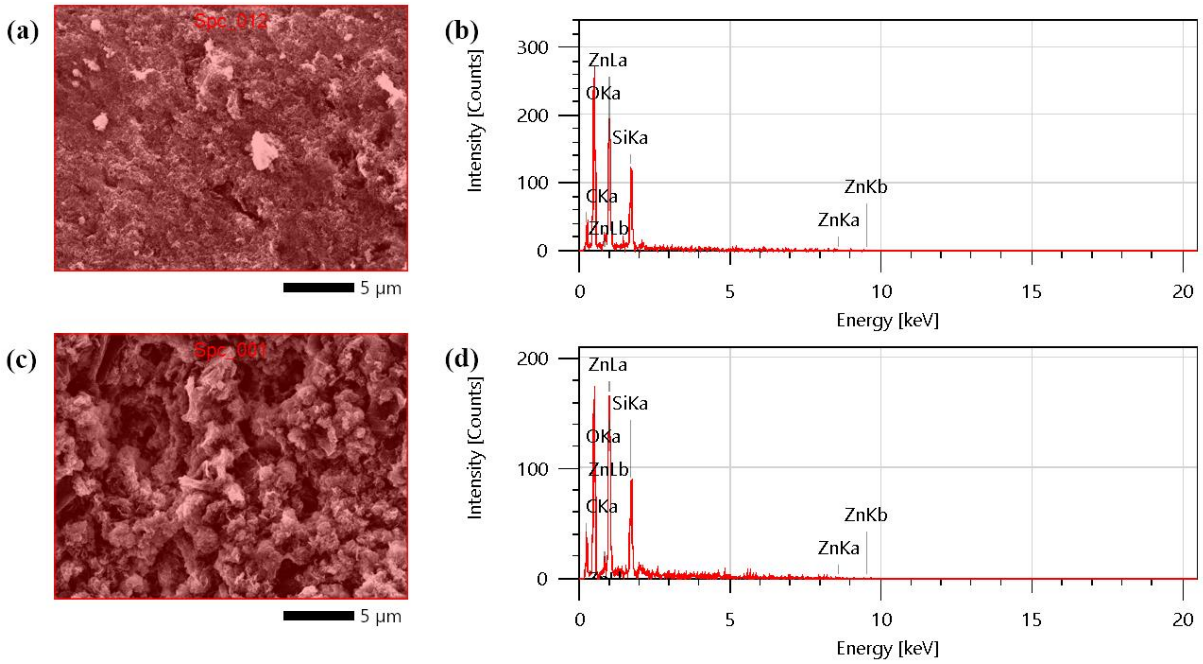

Figure 4: SEM-EDS analysis. SEM image (a) and EDS spectrum (b) of the analyzed area in GO-SG-ZH powder. SEM image (c) and EDS spectrum (d) of the analyzed area in GO-SG-ZH hydrogel.

Table 2: EDS analysis of elemental compostions of GO-SG-ZH derived from the powder and hydrogel.

Materials	C (at%)	O (at%)	Si (at%)	Zn (at%)
GO-SG-ZH powder	18.78 ± 1.22	57.53 ± 2.03	12.64 ± 0.84	11.04 ± 0.58

GO-SG-ZH hydrogel	23.66 ± 1.59	51.90 ± 2.30	11.63 ± 0.95	12.81 ± 0.73

EDS analysis in Figure 4 and Table 2 discloses the elemental compositions of as-prepared GO-SG-ZH powder and hydrogel. Accordingly, atomic proportions of carbon, oxygen, silicon and zinc elements in both nanocomposites are relatively similar. Theoretical contents of SiO_2 and $Zn(OH)_2$ in GO-SG-ZH nanocomposite powder are estimated to be 37.92% and 33.12% respectively, so the remaining content of GO nanosheets is about 28.96%. Similarly, SiO_2, $Zn(OH)_2$ and GO contents derived from GO-SG-ZH hydrogel are calculated to be 34.89%, 38.43% and 26.68% respectively. SEM-EDS elemental mapping of three-dimensional structure of GO-SG-ZH hydrogel is given in Supporting information Figure S1.

Crystallography, functional group, aqueous dispersibility and hydration lubrication

Dry powder of GO-SG-ZH nanocomposite was analyzed using XRD and FTIR methods. In Figure 5a, the XRD pattern exhibited sharp characteristic peaks of $Zn(OH)_2$ crystal at $2\theta = 20.2^o$, 20.94^o, 25.07^o, 27.23^o, 27.83^o and 32.97^o [41-43]. Zinc hydroxide nanoscrystals (ZH) were formed on the nanocomposite during the precipitation by alkaline ammonia in the synthesis (see Methods section). The constituents of GO and SG nanomaterials had amorphous structures that did not give obvious peaks in the XRD pattern. Regarding FTIR spectrum in Figure 5b, most of obvious peaks are attributed to functional groups of nanosilica. The vibration band at 3772.1 cm^{-1} is assigned to silanol groups on nanosilica surface (Si-OH). The bands at 3405.7 cm^{-1} and 1628.6 cm^{-1} are characteristic of stretching mode and bending mode of water molecules adsorbed on the surface [44]. The bands at 1017.3 cm^{-1} and 464.8

cm^{-1} represent the stretching vibrations of siloxane groups (Si-O-Si). Particularly, the FTIR band at 662.43 cm^{-1} is attributed to the bending vibration of Zn-O-Si bonds in GO-SG-ZH nanocomposite [45].

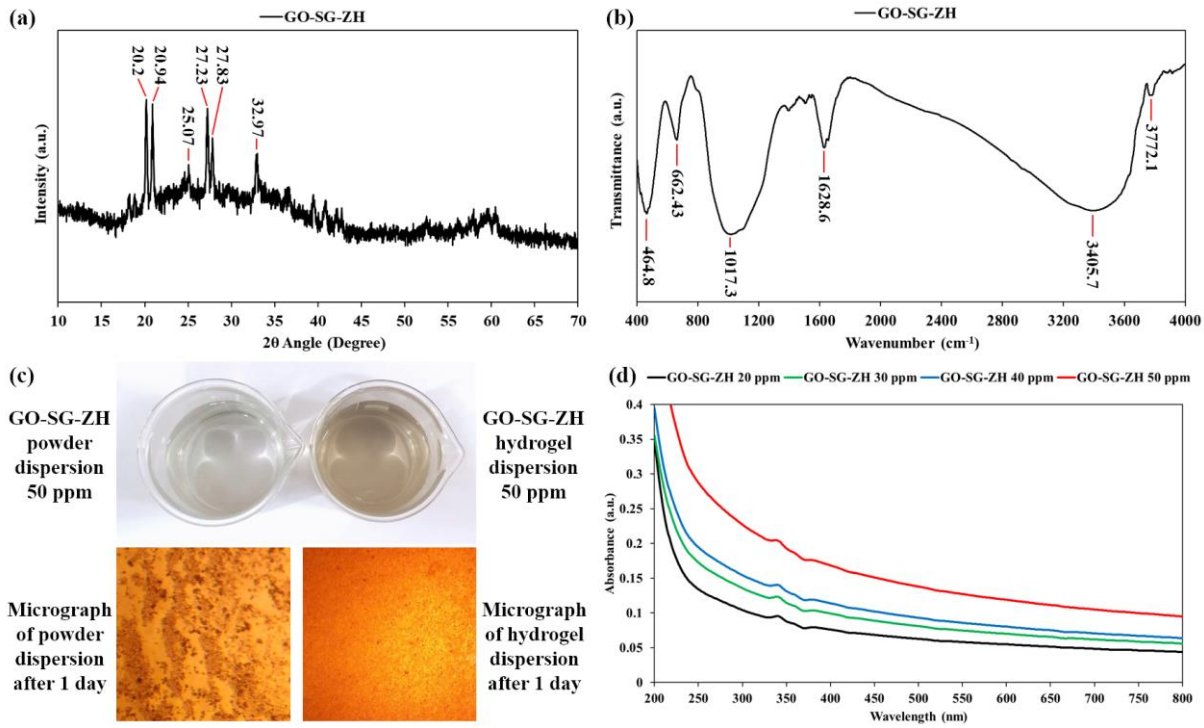

Figure 5: (a) XRD pattern of GO-SG-ZH powder. (b) FTIR spectrum of GO-SG-ZH powder. (c) Aqueous dispersions of GO-SG-ZH powder and hydrogel (concentrations of 50 ppm) and their sedimented particles after 1 day (visualized by the optical microscope). (d) UV-Vis spectra of aqueous dispersions of GO-SG-ZH hydrogel.

Supramolecular systems with non-covalent interactions and reversible crosslinks are recognized to provide extraordinary properties and applications [38-40]. Reversible self-assembly is an advantage of supramolecular graphene-based hydrogel in comparison with the powder form [13-16]. Hydration layers in between graphene-based sheets not only reduce intersheet binding energy (van der Waals force) but also generate repulsive forces for exfoliating the macroscopic assembly into nanoscale structures especially under external stimulations like sonication and mechanics. Reversible self-assembly of graphene-based nanosheets in water is essential to many

applications, such as adsorption, photocatalysis, biosensing, drug delivery, aqueous paints and multifunctional coatings [46-48]. Figure 5c exhibits the aqueous dispersions derived from the sonication of GO-SG-ZH hydrogel and powder in water (see Supporting Information Figure S2). Ultrasound waves vibrated water molecules and created cavitation in the hydrogel structure, leading to the exfoliation of graphene-based nanosheets in water environment. It is notable that low concentrations (≤ 50 ppm) are necessary to obtain homogenous dispersions. The ultrasonic dispersion of GO-SG-ZH hydrogel was faster and clearer due to the high content of water intercalation. GO-SG-ZH powder contained about 10% water and approximate 60% nanosilica and zinc hydroxide nanoparticles that functioned as spacing layers between graphene-based nanosheets. Therefore, the ultrasonic treatment of GO-SG-ZH powder in water also gave homogeneous dispersion. However, the aqueous dispersion of GO-SG-ZH powder was not completely exfoliated in the aqueous environment and settled down quickly. Stacked agglomerates of GO-SG-ZH powder at the bottom of the dispersion were observed in the micrograph in Figure 5c, while the micrograph of the dispersion of GO-SG-ZH hydrogel showed no big particles of agglomerated nanomaterials. In Figure 5d, UV-Vis spectra of aqueous dispersions of GO-SG-ZH hydrogel present the light absorptions in ultraviolet range (200 – 400 nm) that were proportional to the colloidal concentrations (50, 40, 30 and 20 ppm). Small absorption peaks at 340 nm and 360 nm correspond to nanosilica and zinc hydroxide nanoparticles respectively [21,41]. In addition, hydration lubrication in supramolecular graphene-based hydrogel is important to applications in paints and coatings [49,50]. While GO-SG-ZH powder could not be directly used for brush painting, GO-SG-ZH hydrogel can be easily coated on various substrates using a simple brush. In scientific literature, it is elucidated that water layers between graphene-based nanosheets significantly alleviate the interfacial frictions of the nanomaterials [51-53]. In this study,

hydration lubrication makes supramolecular graphene-based hydrogels suitable for direct brush coating on PLA films.

Light transmittance spectroscopy, microscopic structure and elemental composition of graphene oxide – nanosilica – zinc hydroxide coating on polylactide film

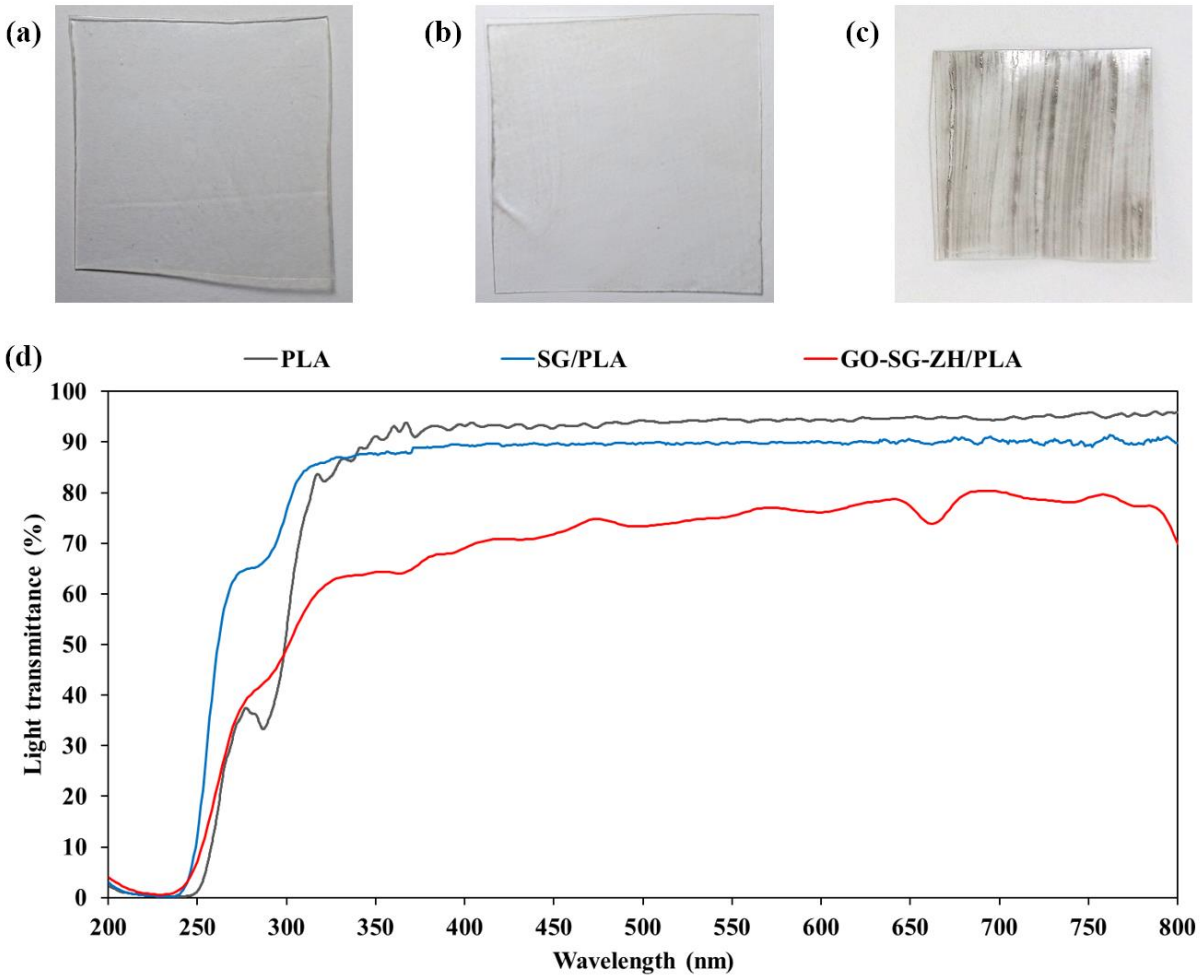

Figure 6: (a) A blank polylactide film (PLA). (b) A polylactide film coated with nanosilica (SG/PLA). (c) A polylactide film coated with graphene oxide – nanosilica – zinc hydroxide (GO-SG-ZH/PLA). (d) Light transmittance spectroscopy of the thin films of PLA, SG/PLA and GO-SG-ZH/PLA.

Hydrogels of nanosilica (SG hydrogel) and graphene oxide – nanosilica – zinc hydroxide (GO-SG-PLA hydrogel) were ultilized as aqueous paints for brush coating

on PLA films. After drying, thin coatings of SG and GO-SG-PLA were formed on the plastic substrates. About apprearance, while blank PLA film was clearly transparent (Figure 6a), SG/PLA film was slightly opaque (Figure 6b) and GO-SG-ZH/PLA film was stripy with black lines of GO color (Figure 6c). Light transmittance spectra in Figure 6d show the transparency levels of the plastic films. In the visible light range of 400 – 700 nm, the average light transmittance values of blank PLA film, SG/PLA film and GO-SG-ZH/PLA film are 94%, 90% and 75% respectively. The SG coating made the transparency decrease of 4%, and the GO-SG-ZH coating resulted in the transparency decline of 19% due to white color of ZH nanoparticles and black color of GO nanosheets.

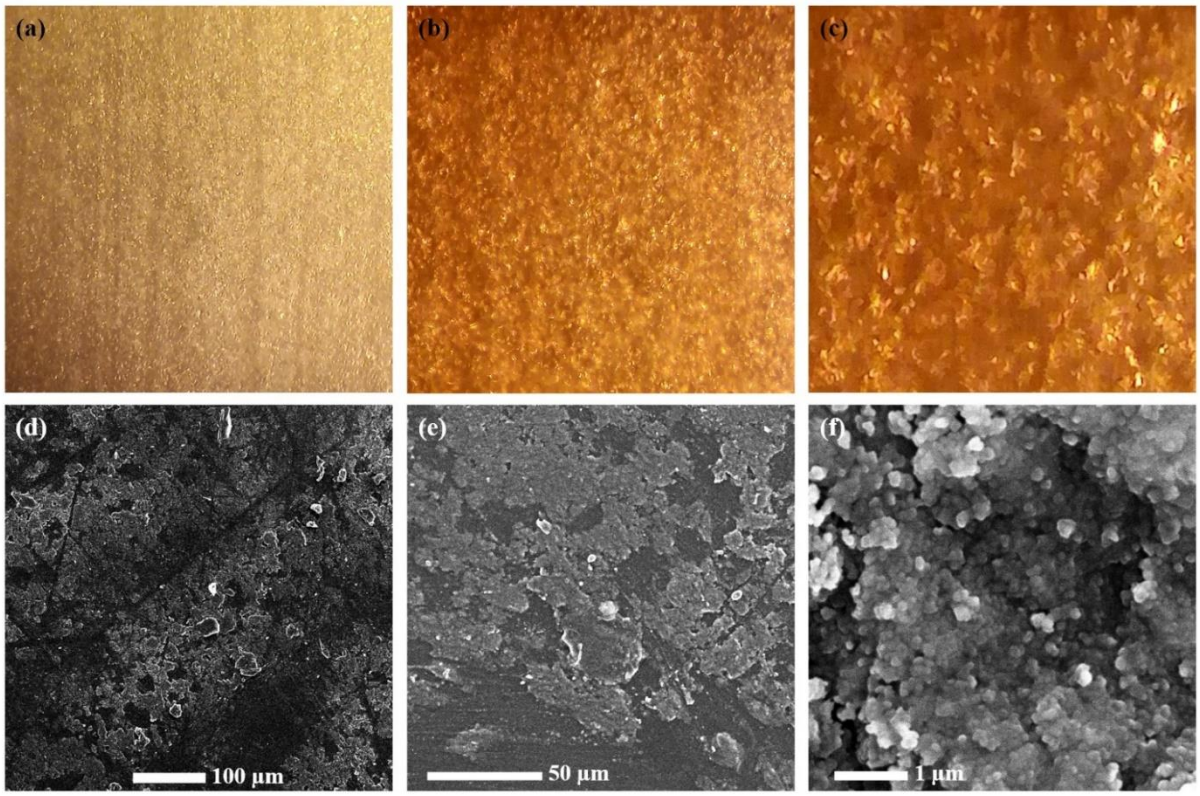

Figure 7: (a, b, c) Micrographs of morphology and structure of a GO-SG-ZH coating on a PLA film. (d, e, f) SEM images of a GO-SG-ZH coating on a PLA film.

Table 3: EDS elemental compostion of the GO-SG-ZH coating on the PLA substrate.

Materials	C (at%)	O (at%)	Si (at%)	Zn (at%)

SG-GO-ZH/PLA film	45.86 ± 1.84	39.64 ± 1.98	8.13 ± 0.70	6.36 ± 0.47

Microscopic structures of the GO-SG-ZH coating on a PLA film were observed and imaged using the optical stereo microscope. Because the PLA substrate was almost transparent, pictures in Figures 7a, 7b and 7c showed GO nanosheets, SG nanoparticles and ZH nanostructures of the GO-SG-ZH coating. Reflected light from the GO-SG-ZH coating gave a three-dimensional vision of coating texture. The nanocomposite coating morphology is pretty uniform. In Figure 7c, two-dimensional shapes of GO nanosheets are obviously visualized. In Figures 7d, 7e and 7f, SEM technique provided higher resolution images of the GO-SG-ZH/PLA film. The brush-coated layer of GO-SG-ZH nanocomposite was not completely uniform since rough coating morphology was observed on the substrate surface. Two-dimensional graphene-based sheets appeared in Figure 7e, and nanoparticles of SG and ZH were shown in Figure 7f. Integrated EDS analysis presented the elemental composition on the surface of GO-SG-ZH/PLA film (Table 3). With the atomic contents of 8.13% silicon and 6.36% zinc, the atomic proportions of SiO_2 and $Zn(OH)_2$ in the nanocomposite were estimated to be 24.39% and 19.08% respectively.

Antibacterial properties of graphene oxide – nanosilica – zinc hydroxide in hydrogel structure and in coating structure

As mentioned in Table 2, solid content of GO-SG-ZH hydrogel was composed of 12.81% zinc atoms as well as 38.43% $Zn(OH)_2$ (derived from ZH constituent). ZH nanoparticles in GO-SG-ZH hydrogel are a good antimicrobial agent that is safe for food packaging and biomedical applications. Antibacterial activity of GO-SG-ZH hydrogel was tested in agar well diffusion assays (Figure 8). The photographic results

showed inhibition zones against *E. coli* bacteria (Figure 8a) and *S. aureus* bacteria (Figure 8b). The inhibition zones resulted from the diffusion of ZH nanoparticles and Zn^{2+} cations from the hydrogel to surrounding agar. As GO-SG-ZH hydrogel is antibacterial, the brush coating of GO-SG-ZH hydrogel on PLA films would produce an antibacterial coating on the substrate.

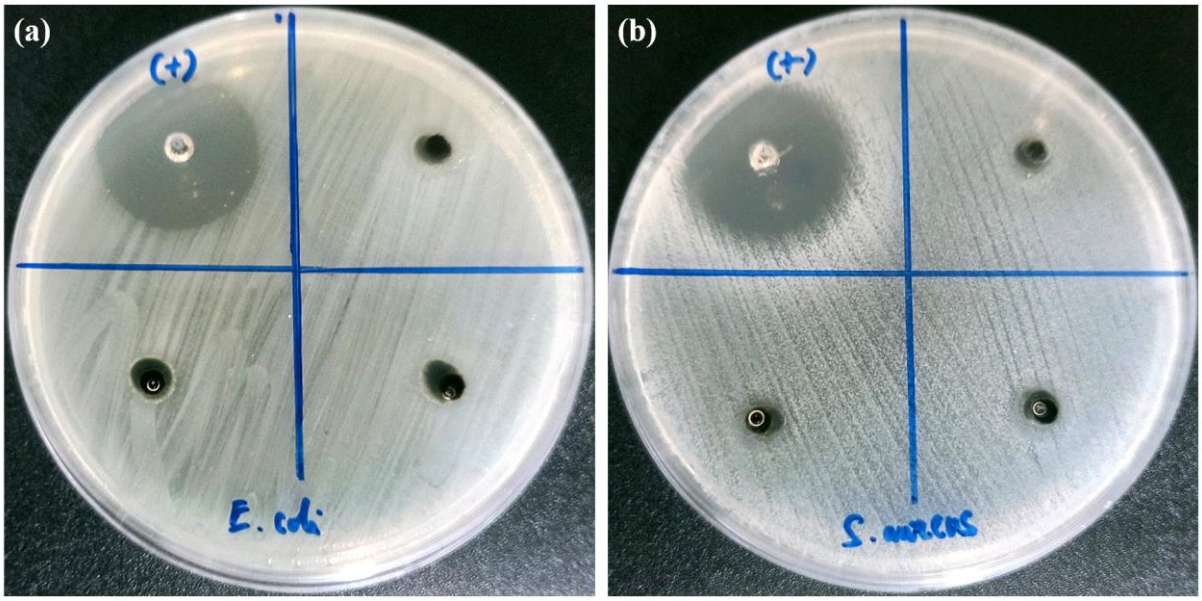

Figure 8: Agar well diffusion assay of GO-SG-ZH hydrogel presents the antibacterial activities of GO-SG-ZH hydrogel againts *E. coli* bacteria (a) and against *S. aureus* bacteria (b).

Antibacterial tests of uncoated and coated PLA films are described in Figure 9 that visualized the interfaces between PLA films and agar/*E. coli* plates. Before incubation process, *E. coli* bacteria did not grow to biofilms (Figures 9a, 9b and 9c). After the incubation at 37°C for 24 hours, stripy biofilms of *E. coli* bacteria were formed on the agar plates (Figures 9d, 9e and 9f). While stripy patterns were observed in the areas of blank PLA film (Figure 9d) and SG/PLA film (Figure 9e), GO-SG-ZH/PLA film presented an inhibition zone at the vicinity of its boundary (Figure 9f). PLA and SG/PLA were not antibacterial materials. Thanks to antibacterial ZH constituent, GO-SG-ZH coating was effective against the growth of *E. coli* biofilm on the coating surface. The

antibacterial result is meaningful for preventions of biofilm formation and surface-mediated infections [14,25,54]. GO-SG-ZH/PLA is a good material for packaging and biomedical applications thanks to its antibiofilm, safety and biodegradability.

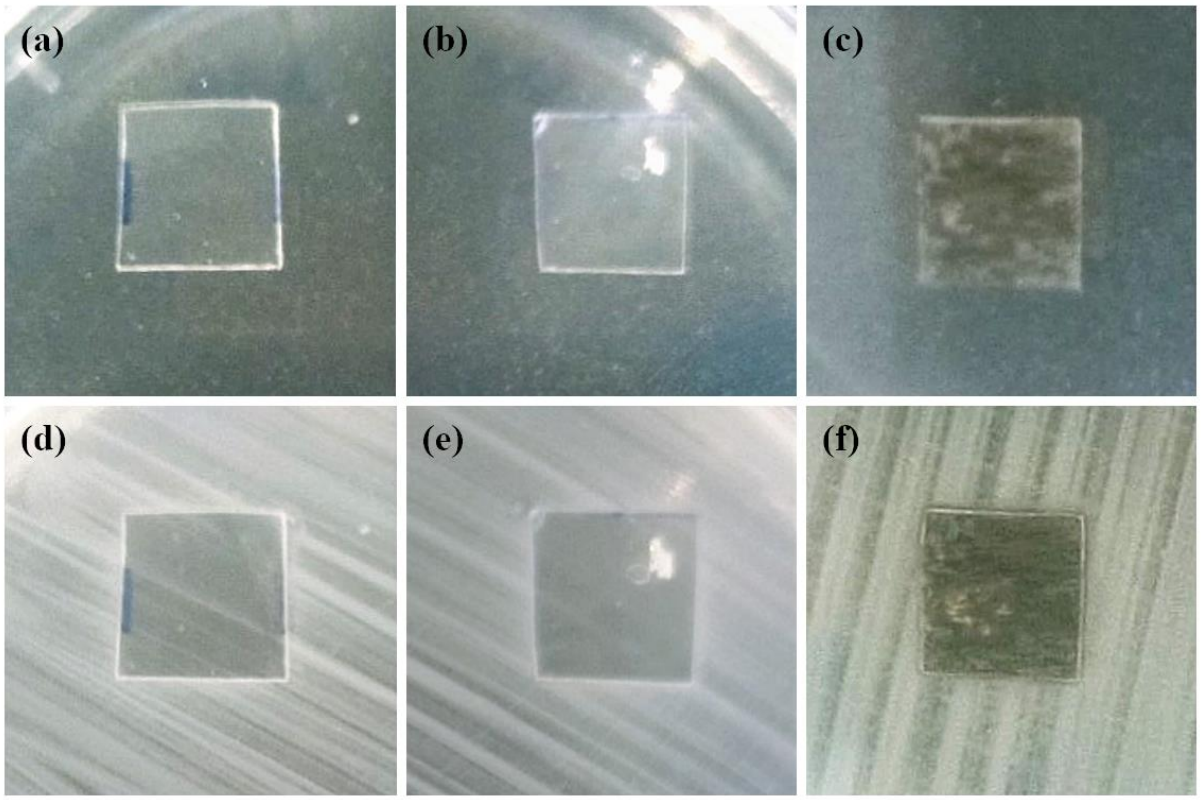

Figure 9: Antibacterial test of uncoated and coated PLA films against the growth of *E. coli* biofilm. (a, b, c) Pictures of a PLA film (a), a SG/PLA film (b) and a GO-SG-ZH/PLA film (c) on agar plates inoculated with *E. coli* bacteria (before incubation). (d, e, f) Pictures of the PLA film (d), SG/PLA film (e) and GO-SG-ZH/PLA film (f) on the agar/biofilm plates after incubation at 37^{o}C for 24 hours.

Stability of graphene oxide – nanosilica – zinc hydroxide coatings on polylactide films in aqueous environments

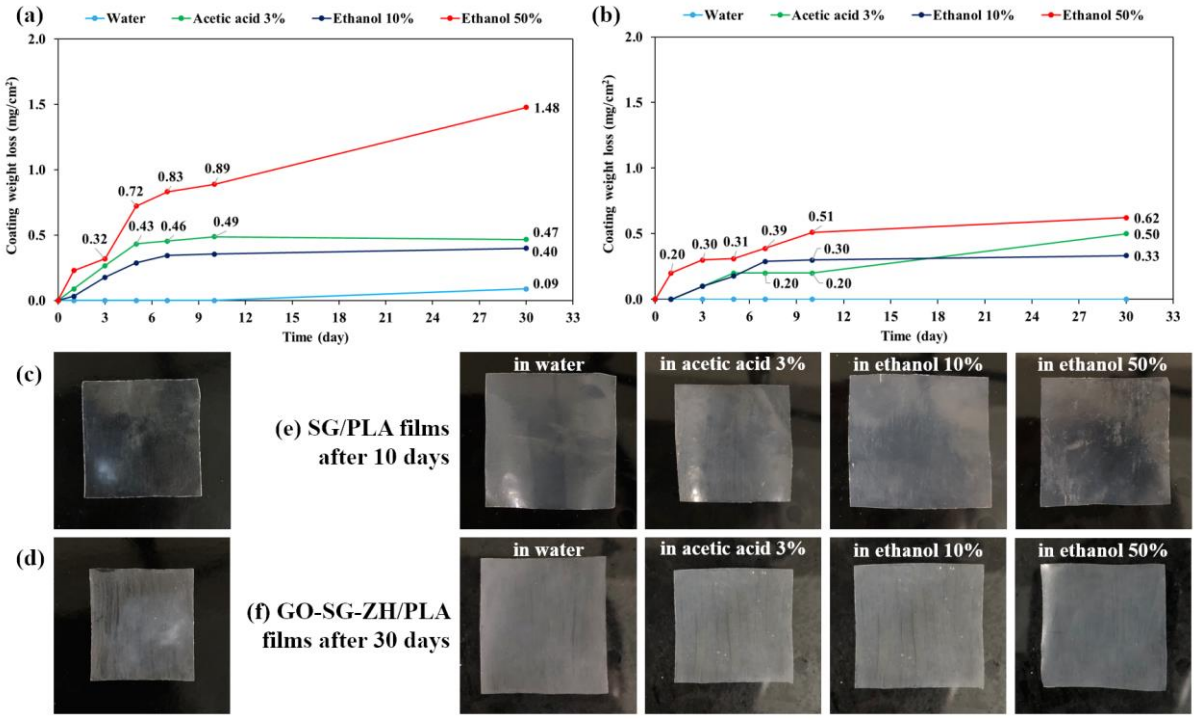

Figure 10: Stability testing of SG/PLA and GO-SG-ZH/PLA films in aqueous food simulants (water, acetic acid 3%, ethanol 10% and ethanol 50%). (a, b) Graphs of weight losses of SG coating (a) and GO-SG-ZH coating (b) in the period of 30 days in the aqueous solutions. (c, d) Initial SG/PLA film (c) and GO-SG-ZH/PLA film (d). (e, f) Pictures of SG/PLA films after 10 days (e) and GO-SG-ZH/PLA films after 30 days (f) in the aqueous environments.

SG/PLA and GO-SG-ZH/PLA films were immersed in aqueous food simulants for one month. The stability of the coatings in aqueous environments was measured by calculating the loss of coating weights. These experimental tests are useful for studying packaging materials and chemical releases over a time period in food simulant environments [14,27]. Line charts in Figure 10 report the weight losses of SG coating (Figure 10a) and GO-SG-ZH/PLA coating (Figure 10b) after 1, 3, 5, 7, 10 and 30 days in the aqueous solutions of water, acetic acid 3%, ethanol 10% and ethanol 50%. Both coatings were quite stable in pure water as the weight losses were insignificant even after 30 days. However, acidic and alcoholic solutions gave more notable effects on

the coatings stability. Especially, the weight losses of SG coating in ethanol 50% were 0.32 mg/cm^2 after 3 days and 1.48 mg/cm^2 after 30 days. The high coating weight loss indicated that the coating of silica nanoparticles was not stable in ethanol solution 50% (equivalent to fatty food environment). Besides, the coating of GO-SG-ZH nanocomposite showed the weight losses of 0.3 mg/cm^2 after 3 days and 0.62 mg/cm^2 after 30 days in ethanol 50%. Although the coating weight losses were considerable in the first 3 days, the trend curve became steady in the period from 3 days to 30 days. The GO-SG-ZH coating was much more stable than SG coating on PLA films. As the coatings of nanosilica and zinc hydroxide nanoparticles were not stable in the alcoholic solution, the coating stability was attributed to graphene-based nanosheets. Large surface area of GO nanosheets is important to crosslinking of nanomaterials in the coating network. Van der Waals interaction at the interface of graphene-based nanosheets contributes to the structural stability. The adhesion of graphene-based nanosheets on the PLA substrate through van der Waals force is another reason for the enhanced stability of GO-SG-ZH/PLA film in the aqueous food simulants.

Mechanical properties of polylactide films with nanosilica-based and graphene-based coatings

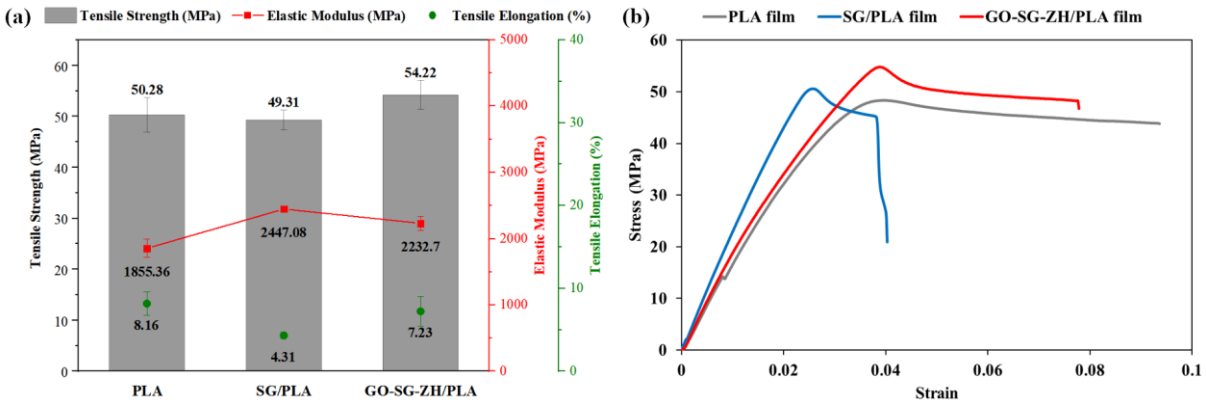

Figure 11: (a) Graph of tensile strength, elastic modulus and tensile elongation. (b) Typical stress – strain curves of PLA film, SG/PLA film and GO-SG-ZH/PLA film.

Table 4: Mechanical properties of blank PLA, SG/PLA and GO-SG-ZH/PLA thin films.

Materials	Tensile strength (MPa)	Elastic modulus (MPa)	Tensile elongation (%)
PLA	50.28 ± 3.4	1855.36 ± 138.56	8.16 ± 1.43
SG/PLA	49.31 ± 1.93	2447.08 ± 27.71	4.31 ± 0.36
GO-SG-ZH/PLA	54.22 ± 2.86	2232.7 ± 105.52	7.23 ± 1.77

Thin coatings bring some effects on the mechanical properties of the plastic films. Tensile testing results of blank PLA, SG/PLA and GO-SG-ZH/PLA films are described in Figure 11 and and summarized in Table 4. Additional data of measurement values and stress – strain curves are given in Supporting Information Table S1, Figure S3, Table S2 and Figure S4. Our previous paper presented that graphene-based coating led to an increase of elastic modulus and a decrease of tensile elongation [14]. Similar trends were also noted in the tensile properties of coated PLA films in this study. Elastic moduli of SG/PLA film and GO-SG-ZH/PLA film rose to 2447.08 ± 27.71 MPa and 2232.7 ± 105.52 MPa, which were 31.89% and 20.34% higher than that of blank PLA film. Nanosilica and graphene-based nanosheets were strong nanostructures that reinforce PLA films. High elasticity of SG and GO-SG-ZH coatings led to the increases in elastic modulus of the nanocomposite films. However, considerable declines of elongation were observed due to the propagation of cracks from the coatings to the substrate. Besides, tensile strength of GO-SG-ZH/PLA film (54.22 ± 2.86 MPa) was slightly higher than that of blank PLA film. It is explained that GO-SG-ZH coating was a stable structure that absorded tensile stress transferred from PLA substrate. With effective stress distribution in the structure, the nanocomposite film had better tensile

strength. Supporting Information Figure S5 shows SEM images of surfaces at the fracture of a GO-SG-ZH/PLA film generated by the tensile measurement.

Conclusion

Supramolecular graphene-based hydrogels are bioinspired structures that are biomimetic to natural hydration structures of cellular membranes, proteins and other biomolecules. While hydration shells participate in the shaping and dynamics of biological structures, water intercalation in graphene-based hydrogels is proposed to reduce intersheet van der Waals interaction, generate repulsive hydration force and facilitate hydration lubrication of graphene-based nanosheets. DFT calculations presented that a water layer in AB bilayer graphene enlarges the intersheet distance from 3.459 Å to 6.626 Å and consequently leads to the reduction of 37.5% in intersheet binding energy of van der Waals force. Theoretically, the first water shell would be crucially responsible for primary hydration force for repulsing the materials stacking. Additionally, hydration lubrication is another interesting effect of water-intercalated graphene-based systems. As graphene-based nanosheets in hydrogel structure are in non-stacking state, they can slide on each other with water lubrication and low interfacial friction. In our experiments, green chemistry approaches were used to synthesize graphene oxide (GO), nanosilica (SG) and graphene oxide – nanosilica – zinc hydroxide nanocomposites (GO-SG-ZH). The green chemistry saved chemical reagents and production energy, converted rice hush ash waste into nanosilica, improved products quality and contributed to environmental sustainability. Especially, the GO-SG-ZH hydrogel is a supramolecular hydration structure with the advantages of reversible self-assembly for aqueous dispersibility, antibacterial activity and brush coating. The brush painting of GO-SG-ZH hydrogel on PLA films resulted in

antibacterial and stable coatings. After hydration in the GO-SG-ZH coating was evaporated, the graphene-based materials adhered to the plastic substrate through van der Waals interaction. Therefore, the nanocomposite coating was stable in aqueous environments and also reinforced the mechanical tensile properties of GO-SG-ZH/PLA films. In summary, supramolecular hydration structure of graphene-based hydrogels is a promising prospective nanotechnology to advance nanoscale structures and interfacial properties for a variety of applications.

Acknowledgements

The authors would like to acknowledge the research collaborations of Fundamental Materials Science Laboratory and Multifunctional Materials Laboratory (Faculty of Materials Science and Technology, University of Science, Vietnam National University Ho Chi Minh City), Laboratory for Computational Physics (Institute for Computational Science and Artificial Intelligence, Van Lang University) and Faculty of Physics (School of Education, Can Tho University).

Author Contributions

Hon Nhien Le: Conceptualization, Investigation, Data curation, Methodology, Formal analysis, Supervision, Visualization, Writing – original draft, Writing – review and editing. Duy Khanh Nguyen: Computational calculations of density functional theory, Manuscript review and editing. Minh Triet Dang: VASP software resources, Manuscript review. Huyen Trinh Nguyen: Synthesis of nanomaterials and thin films. Thi Bang Tam Dao: Data curation, Resources. Trung Do Nguyen: Instrumentation, Resources. Chi Nhan Ha Thuc: Supervision, Validation, Manuscript review. Van Hieu Le: Supervision, Investigation, Validation, Manuscript review and editing.

ORCID

Hon Nhien Le - https://orcid.org/0000-0001-5397-7665

Data Availability Statement

Supporting data for the findings in this study is available from the corresponding author upon request.

References

1. Chaplin, M. Do we underestimate the importance of water in cell biology?; Nat. Rev. Mol. Cell. Biol. 2006, 7, 861–866. https://doi.org/10.1038/nrm2021
2. Bellissent-Funel, M. C.; Hassanali, A.; Havenith, M.; Henchman, R.; Pohl, P.; Sterpone, F.; van der Spoel, D.; Xu, Y.; Garcia, A. E. Water Determines the Structure and Dynamics of Proteins; Chem. Rev. 2016, 116, 13, 7673–7697. https://doi.org/10.1021/acs.chemrev.5b00664
3. Laage, D.; Elsaesser, T.; Hynes, J. T. Water Dynamics in the Hydration Shells of Biomolecules; Chem. Rev. 2017, 117, 10694−10725. https://doi.org/10.1021/acs.chemrev.6b00765
4. Konstantinovsky, D.; Perets, E. A.; Santiago, T.; Velarde, L.; Hammes-Schiffer, S.; Yan, E. C. Y. Detecting the First Hydration Shell Structure around Biomolecules at Interfaces; ACS Cent. Sci. 2022, 8, 1404−1414. https://doi.org/10.1021/acscentsci.2c00702
5. Valle-Delgado, J. J.; Molina-Bolívar, J. A.; Galisteo-González, F.; Gálvez-Ruiz, M. J. Evidence of hydration forces between proteins; Curr. Opin. Colloid Interface Sci. 2011, 16, 572–578. https://doi.org/10.1016/j.cocis.2011.04.004

6. Donaldson, E. C.; Alam, W. Chapter 2 - Surface Forces; Wettability; Gulf Publishing Company, 2008, Pages 57-119. https://doi.org/10.1016/B978-1-933762-29-6.50008-9
7. Israelachvili, J. N. Chapter 21 - Interactions of Biological Membranes and Structures; Intermolecular and Surface Forces (Third Edition); Academic Press, 2011, Pages 577-616. https://doi.org/10.1016/B978-0-12-375182-9.10021-1
8. West, A. Chapter 2 - Intermolecular Forces and Solvation; Interface Science and Technology; Academic Press, 2018, Volume 21, Pages 49-130. https://doi.org/10.1016/B978-0-12-801970-2.00002-1
9. Pérez, E. M.; Martín, N. π–π interactions in carbon nanostructures; Chem. Soc. Rev. 2015, 44, 6425-6433. https://doi.org/10.1039/C5CS00578G
10. Luo, J.; Kim, J.; Huang, J. Material processing of chemically modified graphene: some challenges and solutions; Acc. Chem. Res. 2013, 46(10), 2225–2234. https://doi.org/10.1021/ar300180n
11. Li, J.; Ostling, M. Prevention of graphene restacking for performance boost of supercapacitors—A review; Crystals 2013, 3, 163–190. https://doi.org/10.3390/cryst3010163
12. Yang, X.; Zhu, J.; Qiu, L.; Li, D. Bioinspired effective prevention of restacking in multilayered graphene films: Towards the next generation of high-performance supercapacitors; Adv. Mater. 2011, 23, 2833–2838. https://doi.org/10.1002/adma.201100261
13. Le, N. H.; Seema, H.; Kemp, K. C.; Ahmed, N.; Tiwari, J. N.; Park, S.; Kim, K. S. Solution-processable conductive micro-hydrogels of nanoparticle/graphene platelets produced by reversible self-assembly and aqueous exfoliation; J. Mater. Chem. A 2013, 1, 12900. https://doi.org/10.1039/C3TA12735D

14. Le, H. N.; Nguyen, T. B. Y.; Nguyen, D. T. T.; Dao, T. B. T.; Nguyen, T. D.; Ha Thuc, C. N. Sonochemical synthesis of bioinspired graphene oxide–zinc oxide hydrogel for antibacterial painting on biodegradable polylactide film; Nanotechnology 2024, 35, 305601. https://doi.org/10.1088/1361-6528/ad40b8
15. Le, H. N.; Dao, T. B. T.; Nguyen, T. D.; Dinh, D. A.; Ha Thuc, C. N.; Le, V. H. Revisiting oxidation and reduction reactions for synthesizing a three-dimensional hydrogel of reduced graphene oxide; RSC Adv. 2024, 14, 30844. https://doi.org/10.1039/D4RA05385K
16. Le, H. N.; Thai, D.; Nguyen, T. T.; Dao, T. B. T.; Nguyen, T. D.; Tieu, D. T.; Ha Thuc, C. N. Improving safety and efficiency in graphene oxide production technology; J. Mater. Res. Technol. 2023, 24, 4440–4453. https://doi.org/10.1016/j.jmrt.2023.04.050
17. Le, H. N.; Nguyen, H. D.; Do, M. H.; Nguyen, T. M. H.; Nguyen, T. D.; Dao, T. B. T.; Dinh, D. A.; Ha Thuc, C. N. Melt processing of graphene-coated polylactide granules for producing biodegradable nanocomposite with higher mechanical strength; Polym.-Plast. Technol. Mater. 2024, 63(11), 1421-1437. https://doi.org/10.1080/25740881.2024.2335186
18. Varma, R. S. Greener and Sustainable Trends in Synthesis of Organics and Nanomaterials; ACS Sustainable Chem. Eng. 2016, 4, 5866−5878. https://doi.org/10.1021/acssuschemeng.6b01623
19. Mor, S.; Manchanda, C. K.; Kansal, S. K.; Ravindra, K. Nanosilica extraction from processed agricultural residue using green technology; J. Clean. Prod. 2017, 143, 1284-1290. https://doi.org/10.1016/j.jclepro.2016.11.142
20. Razak, N. A. A.; Othman, N. H.; Shayuti, M. S. M.; Jumahat, A.; Sapiai N.; Lau W. J. Agricultural and industrial waste-derived mesoporous silica nanoparticles:

A review on chemical synthesis route; J. Environ. Chem. Eng. 2022, 10, 107322. https://doi.org/10.1016/j.jece.2022.107322

21. Le, H. N.; Dang, T. M. T.; Le, T. T.; Dao, T. B. T.; Nguyen, T. D.; Ha Thuc, C. N. Investigating nanosilica and biocarbon extracted from rice husk ash generated by industrial steam generators; Science & Technology Development Journal: Natural Sciences 2025, in press.
22. Berland, K.; Cooper, V. R.; Lee, K.; Schröder, E.; Thonhauser, T.; Hyldgaard, P.; Lundqvist, B. I. van der Waals forces in density functional theory: a review of the vdW-DF method; Rep. Prog. Phys. 2015, 78, 066501. https://doi.org/10.1088/0034-4885/78/6/066501
23. Grimme, S.; Antony, J.; Schwabe, T.; Muck-Lichtenfeld, C. Density functional theory with dispersion corrections for supramolecular structures, aggregates, and complexes of (bio)organic molecules; Org. Biomol. Chem. 2007, 5, 741–758. https://doi.org/10.1039/b615319b
24. Grimme, S.; Antony, J.; Ehrlich, S.; Krieg, H. A consistent and accurate ab initio parametrization of density functional dispersion correction (DFT-D) for the 94 elements H-Pu; J. Chem. Phys. 2010, 132, 154104. https://doi.org/10.1063/1.3382344
25. Kumar, A.; Vemula, P. K.; Ajayan, P. M.; John, G. Silver-nanoparticle-embedded antimicrobial paints based on vegetable oil; Nat. Mater. 2008, 7, 236–241. https://doi.org/10.1038/nmat2099
26. Nguyen, T. T.; Tran Pham, B. T.; Le, H. N.; Bach, L. G; Ha Thuc, C. N. Comparative characterization and release study of edible films of chitosan and natural extracts; Food Packag. Shelf Life 2022, 32, 1–12. https://doi.org/10.1016/j.fpsl.2022.100830

27. Le, H. N.; Nguyen, L. N. L.; Dao, T. B. T.; Nguyen, T. D.; Ha Thuc, C. N. Highly tough and antibacterial nanocomposite film of poly(vinyl alcohol)/graphene-oxide-ZnO for biomedical application; Int. J. Nanotechnol. 2025, in press.
28. Birowska, M.; Milowska, K.; Majewski, J. A. Van Der Waals Density Functionals for Graphene Layers and Graphite; Acta Phys. Pol. A 2011, 120(5), 845-848.
29. Song, R.; Feng, W.; Jimenez-Cruz, C. A.; Wang, B.; Jiang, W.; Wang, Z.; Zhou, R. Water film inside graphene nanosheets: electron transfer reversal between water and graphene via tight nano-confinement; RSC Adv. 2015, 5, 274. https://doi.org/10.1039/c4ra13736a
30. Rêgo, C. R. C.; Oliveira, L. N.; Tereshchuk, P.; Da Silva, J. L. F. Comparative study of van der Waals corrections to the bulk properties of graphite; J. Phys.: Condens. Matter 2015, 27, 415502. https://doi.org/10.1088/0953-8984/27/41/415502
31. Khan, M. I. H.; Farrell, T.; Nagy, S. A.; Karim, M. A. Fundamental Understanding of Cellular Water Transport Process in Bio-Food Material during Drying; Sci. Rep. 2018, 8, 15191. https://doi.org/10.1038/s41598-018-33159-7
32. Israelachvili, J.; Wennerström, H. Role of hydration and water structure in biological and colloidal interactions; Nature 1996, 379, 219–225. https://doi.org/10.1038/379219a0
33. Liang, Y.; Hilal, N.; Langston, P.; Starov, V. Interaction forces between colloidal particles in liquid: Theory and experiment; Adv. Colloid Interface Sci. 2007, 134–135, 151–166. https://doi.org/10.1016/j.cis.2007.04.003
34. Parsegian, V. A.; Zemb, T. Hydration forces: Observations, explanations, expectations, questions; Curr. Opin. Colloid Interface Sci. 2011, 16, 618–624. https://doi.org/10.1016/j.cocis.2011.06.010

35. Lang, X.; Shi, L.; Zhao, Z.; Min, W. Probing the structure of water in individual living cells; Nat. Commun. 2024, 15, 5271. https://doi.org/10.1038/s41467-024-49404-9

36. Harrellson, S. G.; DeLay, M. S.; Chen, X.; Cavusoglu, A. H.; Dworkin, J.; Stone, H. A.; Sahin, O. Hydration solids, Nature 2023, 619, 500–505. https://doi.org/10.1038/s41586-023-06144-y

37. Huang, H.; Park, H.; Huang, J. Self-crosslinking of graphene oxide sheets by dehydration; Chem 2022, 8(9), 2432-2441. https://doi.org/10.1016/j.chempr.2022.05.016

38. Wang, Y.; Chen, S.; Qiu, L.; Wang, K.; Wang, H.; Simon, G. P.; Li, D. Graphene-Directed Supramolecular Assembly of Multifunctional Polymer Hydrogel Membranes; Adv. Funct. Mater. 2014, 25(1), 126-133. https://doi.org/10.1002/adfm.201402952

39. Zhan, H.; Xiong, Z.; Cheng, C.; Liang, Q.; Liu, J. Z.; Li, D. Solvation-Involved Nanoionics: New Opportunities from 2D Nanomaterial Laminar Membranes; Adv. Mater. 2019, 32(18), 1904562. https://doi.org/10.1002/adma.201904562

40. Ikura, R.; Park, J.; Osaki, M.; Yamaguchi, H.; Harada, A.; Takashima, Y. Design of self-healing and self-restoring materials utilizing reversible and movable crosslinks; NPG Asia Mater. 2022, 14, 10. https://doi.org/10.1038/s41427-021-00349-1

41. Wang, M.; Jiang, L.; Kim, E. J.; Hahn, S. H. Electronic structure and optical properties of $Zn(OH)_2$: LDA+U calculations and intense yellow luminescence; RSC Adv. 2015, 5, 87496. https://doi.org/10.1039/c5ra17024a

42. Otis, G.; Ejgenberg, M.; Mastai, Y. Solvent-Free Mechanochemical Synthesis of ZnO Nanoparticles by High-Energy Ball Milling of ε-$Zn(OH)_2$ Crystals; Nanomaterials 2021, 11, 238. https://doi.org/10.3390/nano11010238

43. Wang, M.; Zhou, Y.; Zhang, Y.; Hahn, S. H.; Kim, E. J. From $Zn(OH)_2$ to ZnO: a study on the mechanism of phase transformation; CrystEngComm 2011, 13, 6024. https://doi.org/10.1039/C1CE05502J

44. Song, X.; Boily, J. F. Water Vapor Adsorption on Goethite; Environ. Sci. Technol. 2013, 47, 7171−7177. https://doi.org/10.1021/es400147a

45. Liu, Y.; Shen, J.; Zhao, L.; Wang, W.; Gong, W.; Zheng, F. Zinc–iron silicate for heterogeneous catalytic ozonation of acrylic acid: efficiency and mechanism; RSC Adv. 2020, 10, 9146. https://doi.org/10.1039/D0RA00308E

46. Su, L.; Sun, J.; Ding, F.; Gao, Y.; Gao, X.; Zheng, L. Molecular insight into the reversible dispersion and aggregation of graphene utilizing photo-responsive surfactants; Appl. Surf. Sci. 2021, 567, 150840. https://doi.org/10.1016/j.apsusc.2021.150840

47. Bepete, G.; Anglaret, E.; Ortolani, L.; Morandi, V.; Huang, K.; Pénicaud, A.; Drummond, C. Surfactant-free single-layer graphene in water; Nat. Chem. 2017, 9, 347–352. https://doi.org/10.1038/nchem.2669

48. Suter, J. L.; Coveney, P. V. Principles governing control of aggregation and dispersion of aqueous graphene oxide; Sci. Rep. 2021, 11, 22460. https://doi.org/10.1038/s41598-021-01626-3

49. Klein, J. Hydration lubrication, Friction 2013, 1(1), 1–23. https://doi.org/10.1007/s40544-013-0001-7

50. Ma, L.; Gaisinskaya-Kipnis, A.; Kampf, N.; Klein, J. Origins of hydration lubrication; Nat. Commun. 2015, 6, 6060. https://doi.org/10.1038/ncomms7060

51. Soler-Crespo, R. A.; Gao, W.; Mao, L.; Nguyen, H. T.; Roenbeck, M. R.; Paci, J. T.; Huang, J.; Nguyen, S. T.; Espinosa, H. D. The Role of Water in Mediating Interfacial Adhesion and Shear Strength in Graphene Oxide; ACS Nano 2018, 12, 6089−6099. https://doi.org/10.1021/acsnano.8b02373

52. Ma, P.; Liu, Y.; Han, K.; Tian, Y.; Ma, L. Hydration lubrication modulated by water structure at TiO_2-aqueous interfaces; Friction 2024, 12, 591–605. https://doi.org/10.1007/s40544-023-0750-x

53. Ge, X.; Chai, Z.; Shi, Q.; Liu, Y.; Wang, W. Graphene superlubricity: A review; Friction 2023, 11, 1953–1973. https://doi.org/10.1007/s40544-022-0681-y

54. Bartoli, M.; Cardano, F.; Piatti, E.; Lettieri, S.; Fin, A.; Tagliaferro, A. Interface properties of nanostructured carbon-coated biological implants: an overview; Beilstein J. Nanotechnol. 2024, 15, 1041–1053. https://doi.org/10.3762/bjnano.15.85